Lipoatrophy and severe metabolic disturbance in mice with fat-specific deletion of PPARγ

Fenfen Wang, Shannon E. Mullican, Joanna R. DiSpirito, Lindsey C. Peed, and Mitchell A. Lazar[1]

Division of Endocrinology, Diabetes, and Metabolism, Department of Medicine, Department of Genetics, and The Institute for Diabetes, Obesity, and Metabolism, Perelman School of Medicine at the University of Pennsylvania, Philadelphia, PA 19104

Edited* by Bruce M. Spiegelman, Dana-Farber Cancer Institute/Harvard Medical School, Boston, MA, and approved October 8, 2013 (received for review August 6, 2013)

Adipose tissue is an important metabolic organ, the dysfunction of which is associated with the development of obesity, diabetes mellitus, and cardiovascular disease. The nuclear receptor peroxisome proliferator-activated receptor gamma (PPARγ) is considered the master regulator of adipocyte differentiation and function. Although its cell-autonomous role in adipogenesis has been clearly demonstrated in cell culture, previous fat-specific knockouts of the murine PPARγ gene did not demonstrate a dramatic phenotype in vivo. Here, using Adipoq–Cre mice to drive adipose-specific recombination, we report a unique fat-specific PPARγ knockout (PPARγ FKO) mouse model with almost no visible brown and white adipose tissue at age 3 mo. As a consequence, PPARγ FKO mice had hugely enlarged pancreatic islets, massive fatty livers, and dramatically elevated levels of blood glucose and serum insulin accompanied by extreme insulin resistance. PPARγ FKO mice also exhibited delayed hair coat formation associated with absence of dermal fat, disrupted mammary gland development with loss of mammary fat pads, and high bone mass with loss of bone marrow fat, indicating the critical roles of adipose PPARγ in these tissues. Together, our data reveal the necessity of fat PPARγ in adipose formation, whole-body metabolic homeostasis, and normal development of fat-containing tissues.

Adipose tissue is an important organ that is critical for whole-body energy and metabolic homeostasis. White adipose tissue (WAT) stores excess energy as lipids, whereas brown adipose tissue (BAT) participates in thermogenesis (1). Adipose tissue also produces various adipokines, which regulate physiology at multiple levels (1). Dysfunction of adipose tissue is closely related to metabolic and cardiovascular diseases (2–6). Indeed, both too much fat (obesity) and too little fat (lipoatrophy or lipodystrophy) lead to insulin resistance and diabetes (3, 5, 7, 8).

In 1994, the nuclear receptor peroxisome proliferator-activated receptor gamma (PPARγ) was identified as the central regulator of adipocyte biology (9–11). Shortly thereafter, PPARγ was identified as the cellular target of antidiabetic thiazolidinedione drugs, implicating this transcription factor as a key player in the maintenance of metabolic homeostasis (12). There are two PPARγ isoforms, γ1 and γ2, which differ only in their amino termini and are both highly expressed in adipocytes (9, 10, 13). Convincing evidence for a critical role of PPARγ in adipogenesis has been mainly derived from cell culture experiments, in which ectopic expression of PPARγ activates adipocyte-specific genes and triggers morphologic adipogenesis (11), whereas PPARγ-null mouse embryonic fibroblasts cannot undergo adipogenesis in vitro (14, 15).

The study of PPARγ function in vivo has been hindered because homozygous deletion of PPARγ is embryonic lethal, due to a defect in placental function (14, 16). Several approaches have been adopted to study the in vivo functions of PPARγ. First, a chimeric rescue strategy was used to demonstrate that PPARγ-null cells cannot contribute to fat formation (17). Additionally, a single viable PPARγ-null pup generated by placental reconstitution exhibited an absence of fat and multiple hemorrhages (16). Furthermore, mice with PPARγ2 absent in the whole body and PPARγ1 largely reduced in WAT had almost no WAT, smaller BAT, mild glucose intolerance, and no fatty liver at the adult stage (18). More dramatic lipodystrophy and insulin resistance were observed in another global PPARγ-deficient mouse model driven by Mox2–Cre with normal liver morphology (19). Finally, dominant-negative mutations in human PPARγ were associated with severe insulin resistance and diabetes mellitus (20). Together, these global PPARγ deletion models suggest that PPARγ is critical for adipose tissue development and whole-body insulin sensitivity.

Cre/loxP strategies for tissue-specific gene deletion have permitted further investigation, and the adipocyte protein 2 promoter-driven Cre line (aP2-Cre) has been used to interrogate the adipose-specific functions of PPARγ in transgenic mice. One such model displayed a progressive but minor reduction in fat mass, with a mild fatty liver (21). Blood glucose, glucose tolerance, and insulin tolerance were normal, but modest insulin resistance was observed on a high-fat diet (HFD) (21). By contrast, a second aP2-Cre–driven PPARγ-deficient mouse line exhibited modest reduction in WAT mass and major loss of BAT, yet improved systemic insulin sensitivity on HFD (22).

Recent studies have underscored the need for caution when interpreting data obtained using aP2-Cre mice (23, 24). This finding, together with the modest phenotypes and contradictory findings about insulin sensitivity in the aP2-Cre–driven adipose PPARγ knockout mouse models, made it of interest to reevaluate the effects of PPARγ deletion in fat. Here we generated a unique fat-specific PPARγ knockout mouse model using a transgenic Cre line driven by the regulatory region of mouse adiponectin (Adipoq–Cre), which has been shown to direct Cre expression in a more specific and efficient manner (23–25). By using this model, fat-specific deletion of PPARγ led to a nearly complete lipoatrophy, accompanied by dramatically impaired

Significance

Obesity, due to increased adipose (fat) tissue, predisposes to metabolic diseases, including diabetes. Thus, it is important to understand adipose development and function. Peroxisome proliferator-activated receptor gamma (PPARγ) is widely believed to be the master regulator of adipocyte biology. Surprisingly, however, previous studies attempting to delete the PPARγ gene specifically in mouse adipose tissue did not demonstrate a dramatic phenotype. By using newer methods, the present study reports that fat-specific loss of PPARγ causes dramatic loss of adipose tissue, severe insulin resistance and diabetes, fatty liver, and abnormalities of bone, skin, and mammary glands, all of which contain adipose tissue. We show that adipocyte PPARγ is required for normal fat development and metabolic function in vivo.

Author contributions: F.W. and M.A.L. designed research; F.W. and L.C.P. performed research; S.E.M. and J.R.D. contributed new reagents/analytic tools; F.W. and M.A.L. analyzed data; and F.W. and M.A.L. wrote the paper.

The authors declare no conflict of interest.

*This Direct Submission article had a prearranged editor.

[1]To whom correspondence should be addressed. E-mail: lazar@mail.med.upenn.edu.

This article contains supporting information online at www.pnas.org/lookup/suppl/doi:10.1073/pnas.1314863110/-/DCSupplemental.

adipokine secretion; massive hepatomegaly; profound insulin resistance and hyperglycemia; and abnormal bone, mammary glands, and skin. These results prove the in vivo necessity of adipose PPARγ for fat formation, whole-body metabolic homeostasis, and normal development of fat-related tissues.

Results

Adipose-Specific PPARγ Deletion in PPARγ Fat-Specific Knockout Mice. Adipoq–Cre mice were crossed to PPARγ floxed (PPARγ f/f) mice to generate fat-specific PPARγ heterozygous mice (Adipoq–Cre, PPARγ f/+) (Fig. S1*A*). To avoid any potential nursing deficiency in female heterozygous mice, male heterozygous mice were bred to female PPARγ f/f to yield the PPARγ fat-specific knockout mice (Adipoq–Cre, PPARγ f/f; referred to as PPARγ FKO), heterozygous (Adipoq–Cre, PPARγ f/+; referred to as PPARγ FHet), and control (PPARγ f/f and PPARγ f/+) littermates (Fig. S1*B*). Pups were born at the expected Mendelian ratio, although a small fraction (~15%) of PPARγ FKO mice died by the time of weaning.

Quantification of mRNA in PPARγ FHet mice demonstrated the expected ~50% reduction of PPARγ expression specifically in inguinal WAT (IWAT), gonadal WAT (GWAT), and BAT but not in control tissues, including liver, muscle, and brain (Fig. 1*A*). Phenotypic evaluation revealed no significant differences in the weights of the whole body and various organs (IWAT, GWAT, BAT, and liver) (Fig. S2 *A* and *B*) or the metabolic profiles [blood glucose, serum insulin, triglyceride (TG), and free fatty acid (FFA) levels] (Fig. S2 *C*–*F*) of 3-mo-old control and PPARγ FHet mice. PPARγ mRNA was more completely deleted in fat (Fig. 1*B*) but not other tissues of the homozygous PPARγ FKO mice, including liver where PPARγ mRNA actually increased, consistent with the marked hepatosteatosis that is described below (Fig. S3). In adipose tissue, both PPARγ protein isoforms were deleted (Fig. 1*C*), as expected, because the *loxP* sites were located on both sides of exons 1 and 2, which are shared by PPARγ1 and PPARγ2. These results demonstrate that the knockout of PPARγ in the PPARγ FKO mouse was fat-specific and efficient.

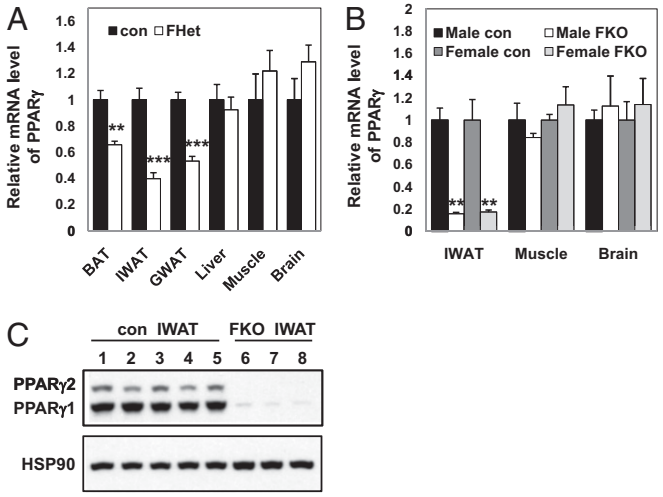

Fig. 1. Specific deletion of PPARγ in adipose tissues. (*A*) PPARγ mRNA level of 3-mo-old control and PPARγ FHet mice in BAT, IWAT, GWAT, liver, muscle, and brain. Values are mean ± SEM (n = 4–5). PPARγ primers are designed to span exon1 and exon2 of PPARγ transcripts, which are targeted for deletion. (*B*) PPARγ mRNA level of 8-d-old control and PPARγ FKO pups in IWAT, muscle, and brain. Values are mean ± SEM (n = 3–4). The same PPARγ primers in *A* are used here. (*C*) Western blot analysis of PPARγ1, PPARγ2, and heat shock protein 90 (HSP90; loading control) in IWAT samples of 8-d-old control and PPARγ FKO pups. For lanes 1–5, each lane includes IWAT sample from individual control pup. For lanes 6–8, each lane includes pooled IWAT samples from two or three PPARγ FKO pups. $^{**}P < 0.01$; $^{***}P < 0.001$ vs. controls.

Severe Lipoatrophy in Adult PPARγ FKO Mice. One-month-old PPARγ FKO mice tended to be of lower body weight than their control littermates, especially in females, but 3-mo-old PPARγ FKO mice reached similar (in males) or even higher (in females) body weights compared with controls (Fig. S4 *A* and *B*). To assess the effects of fat PPARγ deletion in adult mice, examination was performed in 3-mo-old PPARγ FKO and control mice. Remarkably, all adipose depots including GWAT (Fig. 2*A*), interscapular WAT, BAT (Fig. 2*B*), IWAT (Fig. 2*C*), mesenteric (Fig. 2*D*), perirenal (Fig. 2*E*), perivascular (Fig. S5*H*), and pericardial WAT (Fig. S5*I*) were nearly absent in male as well as female (Fig. S5 *A*–*E*) PPARγ FKO mice. Consistent with this dramatic lipoatrophy, serum levels of leptin, resistin, and adiponectin were reduced to near background levels in adult PPARγ FKO mice (Fig. 2 *F*–*H*). Histological analysis of residual tissue collected from 3-mo-old PPARγ FKO mice at locations where adipose tissues would normally be found revealed a small number of adipocytes dispersed among a great number of stromal cells in both IWAT (Fig. 2*I* and Fig. S5*F*) and GWAT (Fig. 2*J* and Fig. S5*G*). These data clearly demonstrate dramatic lipoatrophy at multiple adipose depots in 3-mo-old PPARγ FKO mice.

Hepatosteatosis and Extreme Insulin Resistance in Adult PPARγ FKO Mice. Lipoatrophy is often accompanied by hepatic steatosis (8, 26), and, indeed, the livers of 3-mo-old PPARγ FKO mice were pale and massively enlarged (Fig. 2*A* and Fig. S5*A*, yellow arrows), weighing three to four times greater than control livers in both males and females (Fig. 3*A*). Histological staining with H&E (Fig. 3*B*) or Oil Red O (Fig. 3*C*) confirmed substantial lipid accumulation in the livers of PPARγ FKO mice. Serum TG and nonesterified fatty acid levels were also increased (Fig. S6 *A* and *B*).

Adult PPARγ FKO mice were also markedly hyperglycemic (Fig. 3*D*), with serum insulin levels elevated >60-fold compared with controls (Fig. 3*E*), suggesting severe insulin resistance. Consistent with this finding, insulin tolerance tests (ITTs) revealed marked resistance to insulin in 3-mo-old PPARγ FKO mice (Fig. 3*F*). Histological analysis revealed hugely enlarged pancreatic islets in PPARγ FKO mice (Fig. 3*G*). Thus, inactivation of PPARγ in adipose tissue caused lipoatrophy-associated hepatic steatosis and extreme insulin resistance.

Early Development of the PPARγ FKO Phenotype. PPARγ FKO pups were noted to actively nurse, based on their milk-filled stomachs. On the first day after birth, intrascapular BAT was visibly absent in PPARγ FKO pups, compared with the typical well-defined lobules of BAT that were easily identified between the shoulder blades in control pups (Fig. 4*A*). Transverse sections of 1-d-old pups revealed that the presumptive BAT depots of PPARγ FKO mice were largely reduced in size and had very abnormal morphology compared with those of PPARγ FHet littermates (Fig. 4*B*). Closer examination revealed that, whereas PPARγ FHet BAT lobules contained well-arranged uniform brown adipocytes with eosinophilic plurivacuolated cytoplasm and centric nucleus, the PPARγ FKO BAT displayed an abnormal organization pattern of cells with reduced volume of cytoplasm and pleomorphic nuclei, likely representing degenerative BAT adipocytes in newborn PPARγ FKO pups (Fig. 4*C*).

WAT cannot be detected macroscopically at birth in rodents (27), which was the case at 1 d of age in either control or PPARγ FKO mice. At 8 d of age, PPARγ FKO pups were found to have IWAT depots that were visible but dramatically smaller than those of controls (Fig. 5*A* and Fig. S7*A*). In addition, PPARγ FKO pups had a very small amount of interscapular WAT, whereas control pups had substantial interscapular WAT in the same location (Fig. 5*B* and Fig. S7*B*). Examination of the reverse side of interscapular fat depots revealed the expected butterfly-shaped BAT in control pups and the complete loss of BAT in PPARγ FKO pups (Fig. 5*C* and Fig. S7*C*). Another striking observation was the cloudy serum in 8-d-old PPARγ FKO mice (Fig. 5*D*), together with markedly increased serum TG and FFA levels (Fig. 5 *E* and *F*), indicating

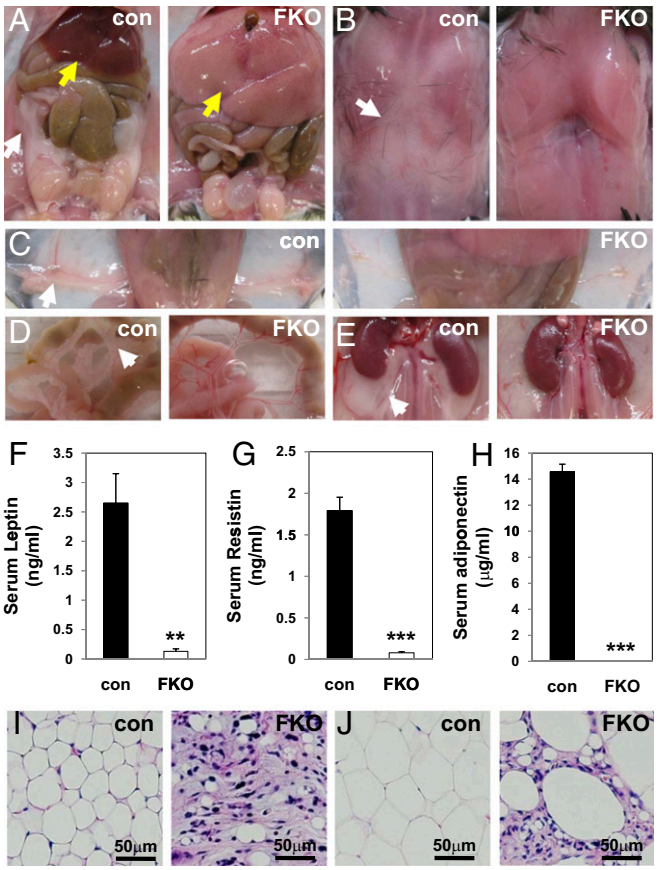

Fig. 2. Severe lipoatrophy in 3-mo-old PPARγ FKO mice. (*A*–*E*) Gross morphology of GWAT (white arrow) and liver (yellow arrow) (*A*), interscapular fat (*B*), IWAT (*C*), mesenteric WAT (*D*), and perirenal WAT (*E*) from 3-mo-old male control and PPARγ FKO mice. (*F*–*H*) Serum leptin (*F*), resistin (*G*), and adiponectin (*H*) levels are shown for 3-mo-old male control and PPARγ FKO mice. Values are mean ± SEM ($n = 3$–6). $^{**}P < 0.01$; $^{***}P < 0.001$ vs. controls. (*I* and *J*) H&E staining of IWAT (*I*) and GWAT (*J*) from 3-mo-old male control and PPARγ FKO mice.

the overflow of excess lipids into blood due to marked reduction of adipose tissues in PPARγ FKO pups.

Histological examination was performed to determine the nature of the small amount of IWAT in the 8-d-old PPARγ FKO mice. Stromal cell density was markedly increased, with interspersed vacuole-containing cells (Fig. 5*G* and Fig. S7*D*). Although most of these cells were much smaller than control adipocytes, immunohistochemical staining for the mature fat cell marker perilipin suggested that these cells were mature adipocytes (Fig. 5*H*). These data support the hypothesis that the failure of adipose tissue accumulation was not due to deficiency in the initiation of adipogenesis in PPARγ FKO fat, which is consistent with the likely occurrence of Adipoq–Cre-mediated PPARγ ablation in relatively mature adipocytes based on the endogenous *Adipoq* gene expression (28). In addition, the vast majority of lipid-laden adipocytes in control fat were positive for PPARγ, whereas the total percentage of PPARγ-positive cells dramatically decreased in PPARγ FKO IWAT (Fig. 5*H* and Fig. S8). These data suggested that mature adipocytes initially formed in PPARγ FKO IWAT, but these perilipin-positive cells had impaired lipid accumulation after Adipoq–Cre-mediated PPARγ depletion.

Furthermore, caspase-3 staining revealed the elevated accumulation of apoptotic cells in PPARγ FKO WAT (Fig. 5*H* and Fig. S8). In addition, increased macrophage infiltration was revealed by F4/80 staining in PPARγ FKO WAT (Fig. 5*H* and Fig. S8), consistent with the inflammatory effects of adipocyte death (29). These findings at 8 d of age suggest that the more severe lipoatrophy observed in 3-mo-old PPARγ FKO mice is due to effects of apoptosis and inflammation over time.

Delayed Coat Formation in PPARγ FKO Mice. PPARγ FKO mice could be easily distinguished from their control littermates because they tended to be skinnier, had lighter-colored rough skin, and had reduced hair growth at 8 d of age (Fig. S9*A*). H&E staining indicated that the skin of PPARγ FKO mice was indistinguishable from that of control littermates at day 1 (Fig. S9*B*). At this time point, there was no obvious lipid accumulation within the skin of either PPARγ FKO or control mice demonstrated by Oil Red O staining (Fig. S9*C*). However, H&E and Oil Red O staining revealed that skin from 8-d-old PPARγ FKO mice contained very few adipocytes and minimal lipid, with less

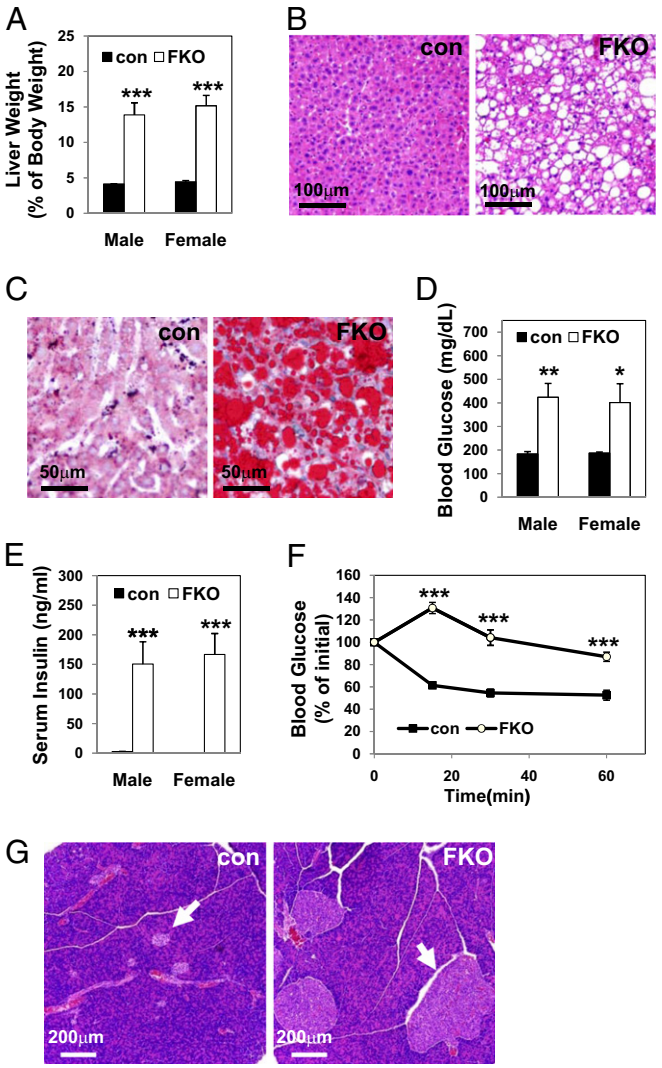

Fig. 3. Massive fatty livers and extreme insulin resistance in 3-mo-old PPARγ FKO mice. (*A*) Liver weights from male or female 3-mo-old control and PPARγ FKO mice. (*B*) H&E staining of livers from 3-mo-old female control and PPARγ FKO mice. (*C*) Oil Red O staining of livers from 3-mo-old female control and PPARγ FKO mice. (*D*) Nonfasting blood glucose levels in 3-mo-old male or female control and PPARγ FKO mice. (*E*) Serum insulin levels in male or female 3-mo-old control and PPARγ FKO mice in nonfasted state. (*F*) ITTs after 4-h fasting in female control and PPARγ FKO mice. (*G*) H&E staining of pancreatic islets (arrows) from 3-mo-old female control and PPARγ FKO mice. Values are mean ± SEM ($n = 4$–5). $^{*}P < 0.05$; $^{**}P < 0.01$; $^{***}P < 0.001$ vs. controls.

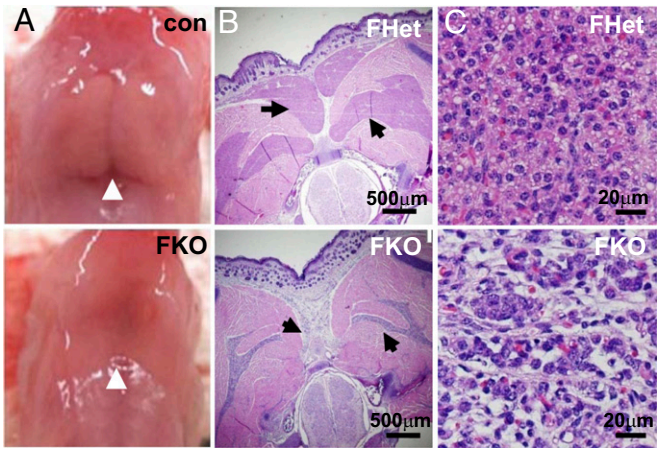

Fig. 4. Ablation of BAT in 1-d-old PPARγ FKO mice. (*A*) Gross morphology of interscapular BAT (arrows) from 1-d-old male control and PPARγ FKO pups. (*B*) H&E staining of transverse sections from the interscapular region of 1-d-old male PPARγ FHet and FKO pups. Different BAT depots are indicated by arrows. (*C*) Microscopic view of BAT depots in *B* with higher magnification.

dense and underdeveloped hair follicles relative to controls (Fig. 6 *A*, *i* and *ii*). Thus, PPARγ FKO mice had delayed coat formation, indicating a critical role of PPARγ in the early stages of hair development. The skin phenotype persisted for up to 1 mo in some PPARγ FKO mice, with most recovering fully by adulthood.

Abnormal Mammary Gland Development in PPARγ FKO Mice. Adipocytes are the predominant component in mammary gland volume and cell number, and they have been shown to play a key role in mammary gland biology (30). In PPARγ FKO mice, the mammary ducts scarcely invaded into the fat pad, and ductal outgrowth was arrested at the prepubertal stage, in contrast to virgin controls (Fig. 6*B*), revealing the necessity of fat PPARγ in ductal formation of mammary glands.

High Trabecular Bone Mass in PPARγ FKO Mice. Tail vertebrae in the 4-mo-old control mice contained highly adipocytic bone marrow, whereas the bone marrow in PPARγ FKO mice was almost adipocyte-free (Fig. 6 *C*, *i*). Osteoblasts and adipocytes are derived from a common mesenchymal stem cell in bone marrow, and interactions between fat and bone are thought to be vital for normal bone integrity (31–33). Three-dimensional images generated by trabecular bone microcomputed tomography (μCT) analysis of the fourth lumbar vertebrae clearly demonstrated increased bone mass in PPARγ FKO mice compared with control mice (Fig. 6 *C*, *ii*). Quantitative analysis confirmed that PPARγ FKO mice had increased bone volume fraction (Fig. S10*A*), trabecular number (Fig. S10*B*), and bone mineral density (Fig. S10*C*). Consistent with this finding, PPARγ FKO mice had a noticeable decrease in trabecular separation (Fig. S10*D*), without a significant difference in trabecular thickness (Fig. S10*E*). Finally, a dramatic decrease in the structure model index revealed a preference for parallel plate formation in PPARγ FKO bones compared with a cylindrical rod model in controls (Fig. S10*F*). Together, these results indicate a critical role for adipose PPARγ in bone biology.

Discussion

Although PPARγ has been unequivocally shown to be necessary for fat cell formation in vitro (11, 15), the role of adipocyte PPARγ in fat depot formation and function in vivo has not been as clear. The present study demonstrates that fat-specific PPARγ ablation leads to severe lipoatrophy, insulin resistance, and other related metabolic disturbances in 3-mo-old PPARγ FKO mice. Moreover, delayed hair coat formation, arrested mammary gland growth, and elevated bone mass in PPARγ FKO mice identify adipose PPARγ as an important regulator of the development and functions of these fat-containing tissues.

Consistent with the essential roles of PPARγ in adipose tissue development proposed by whole-body PPARγ knockout studies (16, 18, 19), BAT and WAT depots, bone marrow fat, and intradermal fat were almost completely absent in 3-mo-old PPARγ FKO mice. This lipoatrophy phenotype in PPARγ FKO mice initiated in both BAT and WAT as early as the first week of life. The dramatic phenotype of these mice is very different from the relatively minor fat reduction (especially WAT) in aP2-Cre–mediated PPARγ-deficient mice (21, 22). This result is likely due to greater effectiveness in Adipoq–Cre-mediated ablation of fat PPARγ (23, 24). The rapid, dramatic, and generalized fat loss in

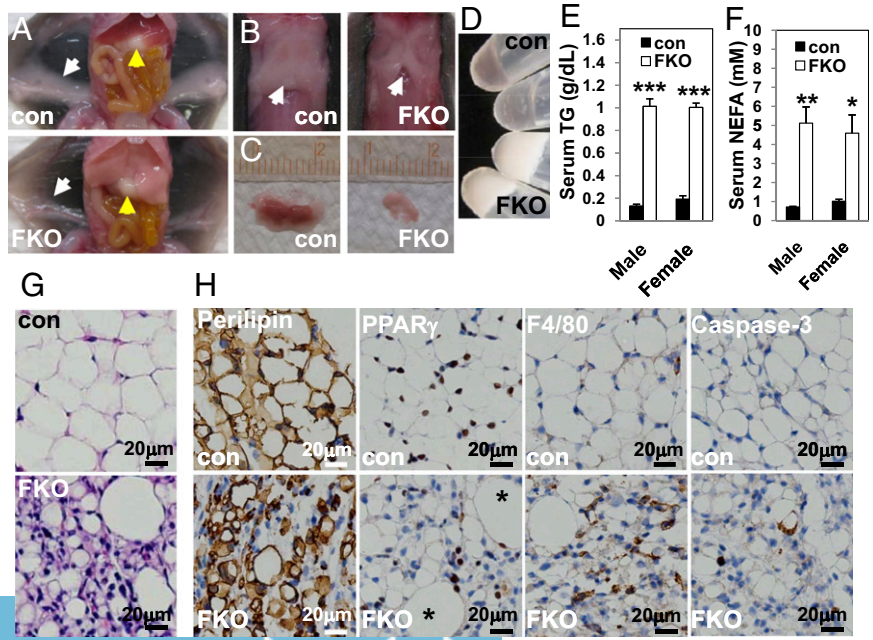

Fig. 5. Loss of WAT, pale liver, and hyperlipidemia in 8-d-old PPARγ FKO pups. (*A*) Exposed ventral view of the 8-d-old male control and PPARγ FKO mice, illustrating the pale liver (yellow arrows) and reduction of IWAT depots (white arrows) in PPARγ FKO pups. (*B*) Exposed dorsal view of interscapular WAT (arrows) in 8-d-old male control and PPARγ FKO mice. (*C*) Flip side of isolated interscapular fat depots in *B* from 8-d-old control and PPARγ FKO pups, demonstrating the absence of BAT in PPARγ FKO pups. (*D–F*) Photographs (*D*) and TG (*E*) and FFA (*F*) levels of the serum samples collected from 8-d-old control and PPARγ FKO pups. Values are mean ± SEM ($n = 3–7$). $^{*}P < 0.05$; $^{**}P < 0.01$; $^{***}P < 0.001$ vs. controls. (*G*) H&E staining of IWAT from 8-d-old male control and PPARγ FKO pups. (*H*) Immunohistochemistry staining of perilipin, PPARγ, F4/80, and caspase-3 proteins in IWAT from 8-d-old male control and PPARγ FKO pups. Two large PPARγ-positive adipocytes are indicated by asterisks.

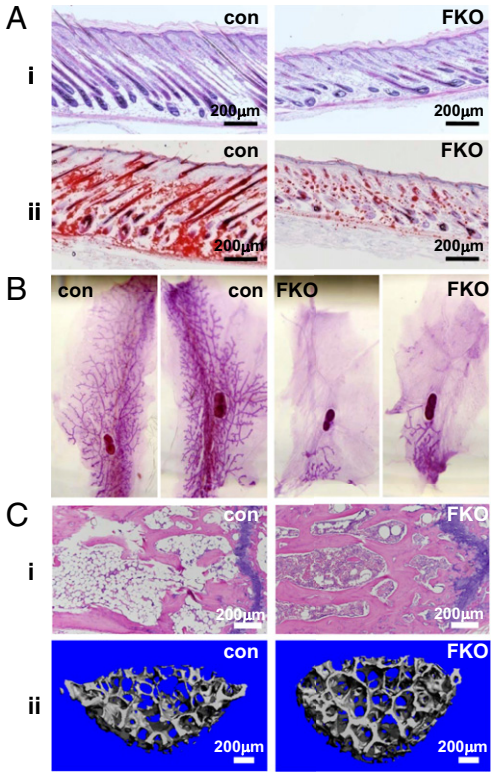

Fig. 6. Delayed hair coat formation, arrested mammary gland development and high bone mass in PPARγ FKO mice. (*A*) H&E (*i*) and Oil Red O (*ii*) staining sections of skin from 8-d-old male control and PPARγ FKO pups. (*B*) Whole-mount analysis of fourth inguinal mammary glands from 4-mo-old female control and PPARγ FKO mice. (*C*) H&E staining sections of tail vertebrae (*i*) and μCT 3D trabecular bone images of fourth lumbar vertebrae (*ii*) from 4-mo-old female control and PPARγ FKO mice.

our PPARγ FKO mice provides direct evidence for the cell-autonomous necessity of PPARγ in healthy fat cell formation in vivo.

Because adiponectin is expressed late in adipogenesis (28), it is likely that Adipoq–Cre-mediated ablation of PPARγ occurs in relatively mature adipocytes, explaining the existence of perilipin-positive adipocytes in the IWAT of 8-d-old PPARγ FKO mice. The perilipin-positive cell population includes some PPARγ-positive cells with large lipid droplets (Fig. 5*H*), as well as a large number of PPARγ-negative cells with tiny vacuoles. This finding suggests that the initially formed large mature adipocytes lost lipids and shrank upon PPARγ ablation, causing the lipoatrophy in 1-wk-old PPARγ FKO pups. The more dramatic lipodystrophy in older PPARγ FKO mice likely results from apoptosis and inflammation, consistent with the pivotal roles of PPARγ in adipocyte function and survival previously revealed by a transient PPARγ knockout mouse model that also noted cellular necrosis (34).

The extreme insulin resistance, massive hepatomegaly, and steatosis are consistent with other models of lipoatrophy-associated diabetes, both in mice and humans (7, 8, 26). It is worth pointing out that the blood glucose is markedly elevated despite hyperplastic pancreatic islets generating a >60-fold increase in insulin levels, suggesting that insulin resistance, rather than failure to produce copious amounts of insulin, is the primary cause of hyperglycemia in this model. This finding is strikingly different from the unchanged insulin sensitivity on normal chow in both or even improved insulin sensitivity on HFD in one of aP2-Cre–mediated PPARγ-knockout mice (21, 22). Thus, the PPARγ FKO mice provide a valuable reagent to investigate not only the net effects of efficient fat-specific PPARγ ablation, but also alterations in glucose homeostasis in severe insulin resistance.

Besides its central role in lipid and glucose homeostasis, our findings reveal that adipocyte PPARγ is also a key factor in regulating the development of multiple other tissues, including skin, mammary gland, and bone. It was reported previously that targeted deletion of PPARγ in follicular stem cells in mice causes a skin and hair phenotype that emulates scarring alopecia (CA), suggesting a crucial role of PPARγ for healthy pilosebaceous units and that loss of this signaling pathway may be responsible for the pathogenesis of CA (35). However, the potential roles of adipocyte PPARγ in regulating hair follicle biology have not been explored before. The delayed hair coat formation in PPARγ FKO pups demonstrated that adipocyte PPARγ is involved in initial hair follicle growth, potentially through interplay between dermal adipocytes and hair follicle cells, which would be consistent with recent studies showing essential roles of immature adipocyte precursor cells within skin in driving follicular stem cell activation during hair follicle regeneration (36).

With regard to mammary biology, previous studies have mainly focused on the role of PPARγ as a mammary tumor suppressor (37–40). Interestingly, conditional knockout of PPARγ in mammary epithelium did not affect normal mammary development (41). By contrast, we found that adipocyte PPARγ ablation arrested mammary gland growth in 4-mo-old mature virgins, indicating a critical role of PPARγ that is most likely related to a key role of the fat pad in normal mammary gland development, as noted in other animal models of adipocyte ablation (42, 43). The adipocytes could function as a source of lipids, adipokines, and other molecules essential for normal mammary epithelial growth, although adipocyte-to-epithelial transdifferentiation has also been demonstrated in mammary gland (44).

The enhanced bone density of PPARγ FKO mice also sheds light on the role of adipocyte PPARγ in bone remodeling. The whole-body heterozygous PPARγ-deficient mice exhibited high bone mass due to increased osteoblastogenesis (45). Intriguingly, mice with PPARγ deletion in hematopoietic lineage cells (including osteoclasts) but not in mesenchymal lineage cells (including osteoblasts and adipocytes) also developed increased bone mass due to impaired osteoclast differentiation (46). The increased bone mass of PPARγ FKO mice underscores the importance of adipocyte PPARγ in maintaining bone homeostasis. Because osteoblasts and adipocytes are derived from a common mesenchymal precursor (31, 32), a likely mechanism would involve the preferential conversion of these precursors to osteoblasts in the absence of PPARγ. The bone phenotype could also result from local or systemic reduction of adipocyte-secreted molecules following deletion of fat PPARγ, including leptin, which has been identified as a potent inhibitor of bone formation (47, 48).

In summary, the striking phenotypes of PPARγ FKO mice reveal the cell-autonomous necessity of fat PPARγ in healthy adipose tissue formation, whole-body metabolism, and the homeostasis of several other fat-containing tissues. In addition, this mouse model provides a valuable reagent for delineating the functions of mature adipocytes in important physiological processes in the body. Finally, the pancreatic islet expansion in this model may also facilitate the development of novel therapeutic approaches to treat metabolic disorders.

Materials and Methods

Animals. Adipoq–Cre mice were a gift from Evan Rosen (Beth Israel Deaconess Medical Center, Boston, MA). PPARγ f/f mice were obtained from Jackson Labs. Both lines are on a C57BL/6 background. They were maintained on a standard diet under 12-h light/12-h dark cycles and euthanized at approximately Zeitgeber time 10 (5:00 PM) for experiments. Blood glucose concentrations were measured by using a glucometer (OneTouch). For ITTs, insulin (Novolin R; 0.6 U per kg body weight) was injected i.p. after a 4-h fast. Serum TG (Stanbio), total FFA (Wako), insulin (Alpco), and adipokines (Millipore) were measured by using commercial kits. Animal care and use procedures followed the guidelines of the Institutional Animal Care and Use Committee of the University of Pennsylvania in accordance with the guidelines of the National Institutes of Health.

Reverse Transcription-Quantitative PCR. Total RNA was isolated from tissues by using TRIzol (Invitrogen) followed by purification with the RNEasy mini kit (Qiagen). One microgram of purified RNA was used to generate cDNA (Applied Biosystems), and quantitative PCR analysis was performed by using primers listed in Table S1. Amplicons were detected with Power SYBR green master mix (Applied Biosystems). Relative gene expression levels were determined by the standard curve method followed by normalization to the housekeeping gene *36B4*.

Immunoblotting. Primary antibodies for PPARγ (Cell Signaling) and HSP90 (Santa Cruz) were detected by a secondary horseradish peroxidase-conjugated antibody (Sigma) and an enhanced chemiluminescent substrate kit (PerkinElmer Western Lightning).

Histology. Tissues were fixed in 4% (wt/vol) paraformaldehyde, and paraffin-embedded sections were subjected to H&E staining. For Oil Red O staining, fixed tissues were embedded in optimal cutting temperature compound and cryosectioned. Immunohistochemistry staining was performed on paraffin sections with antibodies to perilipin (Cell Signaling), PPARγ (Thermo Scientific), F4/80 (Invitrogen), and caspase-3 (R&D Systems), according to standard protocols. Quantification of immunohistochemistry staining was done by calculating the percentage of specific marker-expressing cells out of total cells from at least 200 cells for each adipose specimen. For whole-mount staining, fixed mammary tissues were stained with carmine alum solution overnight, washed in ethanol, and cleared in xylene.

μCT Analysis. Fixed lumbar vertebrae samples were scanned at a 6-μm resolution by using a specimen μCT system (μCT35; Scanco Medical AG). All parameters were determined by using manufacturer-provided software (Scanco Medical AG).

Statistics. A Student's two-tailed *t* test was performed for all experiments to determine the significance of the differences between two groups.

ACKNOWLEDGMENTS. We thank G. Cotsarelis, Y. Zheng, S. M. Prouty, J. T. Seykora, and the Penn Skin Disease Research Core (Grant SDRC 5-P30-AR-057217) for help with skin histology; E. M. Shore, G. Ramaswamy, X. S. Liu, and W.-J. Tseng from the μCT imaging core (Penn Center for Musculoskeletal Disorders) for help in bone analysis; and H. W. Collins [Radioimmunoassay and Biomarkers Core, Penn Diabetes Research Center; National Institutes of Health (NIH) Grant DK19525] for adipokine measurements. Histology was performed by the Penn Digestive Diseases Center Morphology Core (NIH Grants DK49210 and DK50306) and by D. Martinez and T. Bhatti (Pathology Core Lab, Children's Hospital of Philadelphia). We also thank J. Jager, Z. Sun, and members of the M.A.L. laboratory for helpful discussions. This work was supported by NIH Grant DK49780 (to M.A.L.) and the Cox Institute for Medical Research.

1. Rosen ED, Spiegelman BM (2006) Adipocytes as regulators of energy balance and glucose homeostasis. *Nature* 444(7121):847–853.
2. Ouchi N, Parker JL, Lugus JJ, Walsh K (2011) Adipokines in inflammation and metabolic disease. *Nat Rev Immunol* 11(2):85–97.
3. Guilherme A, Virbasius JV, Puri V, Czech MP (2008) Adipocyte dysfunctions linking obesity to insulin resistance and type 2 diabetes. *Nat Rev Mol Cell Biol* 9(5):367–377.
4. Mathieu P, Lemieux I, Després J-P (2010) Obesity, inflammation, and cardiovascular risk. *Clin Pharmacol Ther* 87(4):407–416.
5. Qatanani M, Lazar MA (2007) Mechanisms of obesity-associated insulin resistance: Many choices on the menu. *Genes Dev* 21(12):1443–1455.
6. Anghel SI, Wahli W (2007) Fat poetry: A kingdom for PPAR gamma. *Cell Res* 17(6): 486–511.
7. Agarwal AK, Garg A (2006) Genetic disorders of adipose tissue development, differentiation, and death. *Annu Rev Genomics Hum Genet* 7:175–199.
8. Garg A, Misra A (2004) Lipodystrophies: Rare disorders causing metabolic syndrome. *Endocrinol Metab Clin North Am* 33(2):305–331.
9. Tontonoz P, Hu E, Graves RA, Budavari AI, Spiegelman BM (1994) mPPAR gamma 2: Tissue-specific regulator of an adipocyte enhancer. *Genes Dev* 8(10):1224–1234.
10. Chawla A, Schwarz EJ, Dimaculangan DD, Lazar MA (1994) Peroxisome proliferator-activated receptor (PPAR) gamma: Adipose-predominant expression and induction early in adipocyte differentiation. *Endocrinology* 135(2):798–800.
11. Tontonoz P, Hu E, Spiegelman BM (1994) Stimulation of adipogenesis in fibroblasts by PPAR gamma 2, a lipid-activated transcription factor. *Cell* 79(7):1147–1156.
12. Lehmann JM, et al. (1995) An antidiabetic thiazolidinedione is a high affinity ligand for peroxisome proliferator-activated receptor gamma (PPAR gamma). *J Biol Chem* 270(22):12953–12956.
13. Zhu Y, Alvares K, Huang Q, Rao MS, Reddy JK (1993) Cloning of a new member of the peroxisome proliferator-activated receptor gene family from mouse liver. *J Biol Chem* 268(36):26817–26820.
14. Kubota N, et al. (1999) PPAR gamma mediates high-fat diet-induced adipocyte hypertrophy and insulin resistance. *Mol Cell* 4(4):597–609.
15. Rosen ED, et al. (2002) C/EBPalpha induces adipogenesis through PPARgamma: A unified pathway. *Genes Dev* 16(1):22–26.
16. Barak Y, et al. (1999) PPAR gamma is required for placental, cardiac, and adipose tissue development. *Mol Cell* 4(4):585–595.
17. Rosen ED, et al. (1999) PPAR gamma is required for the differentiation of adipose tissue in vivo and in vitro. *Mol Cell* 4(4):611–617.
18. Koutnikova H, et al. (2003) Compensation by the muscle limits the metabolic consequences of lipodystrophy in PPAR gamma hypomorphic mice. *Proc Natl Acad Sci USA* 100(24):14457–14462.
19. Duan SZ, et al. (2007) Hypotension, lipodystrophy, and insulin resistance in generalized PPARgamma-deficient mice rescued from embryonic lethality. *J Clin Invest* 117(3):812–822.
20. Barroso I, et al. (1999) Dominant negative mutations in human PPARgamma associated with severe insulin resistance, diabetes mellitus and hypertension. *Nature* 402(6764):880–883.
21. He W, et al. (2003) Adipose-specific peroxisome proliferator-activated receptor gamma knockout causes insulin resistance in fat and liver but not in muscle. *Proc Natl Acad Sci USA* 100(26):15712–15717.
22. Jones JR, et al. (2005) Deletion of PPARgamma in adipose tissues of mice protects against high fat diet-induced obesity and insulin resistance. *Proc Natl Acad Sci USA* 102(17):6207–6212.
23. Mullican SE, et al. (2013) A novel adipose-specific gene deletion model demonstrates potential pitfalls of existing methods. *Mol Endocrinol* 27(1):127–134.
24. Lee KY, et al. (2013) Lessons on conditional gene targeting in mouse adipose tissue. *Diabetes* 62(3):864–874.
25. Eguchi J, et al. (2011) Transcriptional control of adipose lipid handling by IRF4. *Cell Metab* 13(3):249–259.
26. Savage DB (2009) Mouse models of inherited lipodystrophy. *Dis Model Mech* 2(11-12): 554–562.
27. Ailhaud G, Grimaldi P, Négrel R (1992) Cellular and molecular aspects of adipose tissue development. *Annu Rev Nutr* 12:207–233.
28. Hu E, Liang P, Spiegelman BM (1996) AdipoQ is a novel adipose-specific gene dysregulated in obesity. *J Biol Chem* 271(18):10697–10703.
29. Pajvani UB, et al. (2005) Fat apoptosis through targeted activation of caspase 8: A new mouse model of inducible and reversible lipoatrophy. *Nat Med* 11(7):797–803.
30. Hovey RC, Aimo L (2010) Diverse and active roles for adipocytes during mammary gland growth and function. *J Mammary Gland Biol Neoplasia* 15(3):279–290.
31. Takada I, Kouzmenko AP, Kato S (2009) Wnt and PPARgamma signaling in osteoblastogenesis and adipogenesis. *Nat Rev Rheumatol* 5(8):442–447.
32. Kawai M, Devlin MJ, Rosen CJ (2009) Fat targets for skeletal health. *Nat Rev Rheumatol* 5(7):365–372.
33. Fazeli PK, et al. (2013) Marrow fat and bone—new perspectives. *J Clin Endocrinol Metab* 98(3):935–945.
34. Imai T, et al. (2004) Peroxisome proliferator-activated receptor gamma is required in mature white and brown adipocytes for their survival in the mouse. *Proc Natl Acad Sci USA* 101(13):4543–4547.
35. Karnik P, et al. (2009) Hair follicle stem cell-specific PPARgamma deletion causes scarring alopecia. *J Invest Dermatol* 129(5):1243–1257.
36. Festa E, et al. (2011) Adipocyte lineage cells contribute to the skin stem cell niche to drive hair cycling. *Cell* 146(5):761–771.
37. Nicol CJ, et al. (2004) PPARgamma influences susceptibility to DMBA-induced mammary, ovarian and skin carcinogenesis. *Carcinogenesis* 25(9):1747–1755.
38. Yin Y, Yuan H, Zeng X, Kopelovich L, Glazer RI (2009) Inhibition of peroxisome proliferator-activated receptor gamma increases estrogen receptor-dependent tumor specification. *Cancer Res* 69(2):687–694.
39. Skelhorne-Gross G, et al. (2012) Stromal adipocyte PPARγ protects against breast tumorigenesis. *Carcinogenesis* 33(7):1412–1420.
40. Suh N, et al. (1999) A new ligand for the peroxisome proliferator-activated receptor-gamma (PPAR-gamma), GW7845, inhibits rat mammary carcinogenesis. *Cancer Res* 59(22):5671–5673.
41. Cui Y, et al. (2002) Loss of the peroxisome proliferation-activated receptor gamma (PPARgamma) does not affect mammary development and propensity for tumor formation but leads to reduced fertility. *J Biol Chem* 277(20):17830–17835.
42. Couldrey C, et al. (2002) Adipose tissue: A vital in vivo role in mammary gland development but not differentiation. *Dev Dyn* 223(4):459–468.
43. Landskroner-Eiger S, Park J, Israel D, Pollard JW, Scherer PE (2010) Morphogenesis of the developing mammary gland: Stage-dependent impact of adipocytes. *Dev Biol* 344(2):968–978.
44. Morroni M, et al. (2004) Reversible transdifferentiation of secretory epithelial cells into adipocytes in the mammary gland. *Proc Natl Acad Sci USA* 101(48):16801–16806.
45. Akune T, et al. (2004) PPARgamma insufficiency enhances osteogenesis through osteoblast formation from bone marrow progenitors. *J Clin Invest* 113(6):846–855.
46. Wan Y, Chong L-W, Evans RM (2007) PPAR-gamma regulates osteoclastogenesis in mice. *Nat Med* 13(12):1496–1503.
47. Ducy P, et al. (2000) Leptin inhibits bone formation through a hypothalamic relay: A central control of bone mass. *Cell* 100(2):197–207.
48. Elefteriou F, et al. (2004) Serum leptin level is a regulator of bone mass. *Proc Natl Acad Sci USA* 101(9):3258–3263.